Understanding the chlorination mechanism and the chlorine-induced separation performance evolution of polypiperazine-amide nanofiltration membrane

Highlights

- Two self-made PPA NFMs were employed to study their chlorination processes.
- Degradation of PPA NFMs includes chlorine substitution and oxidation of -NH groups.
- Damaged separation performance of chlorinated PPA NFMs can be partially recovered.
- -NH group content change in PPA layer cause the separation performance evolution

Graphical abstract

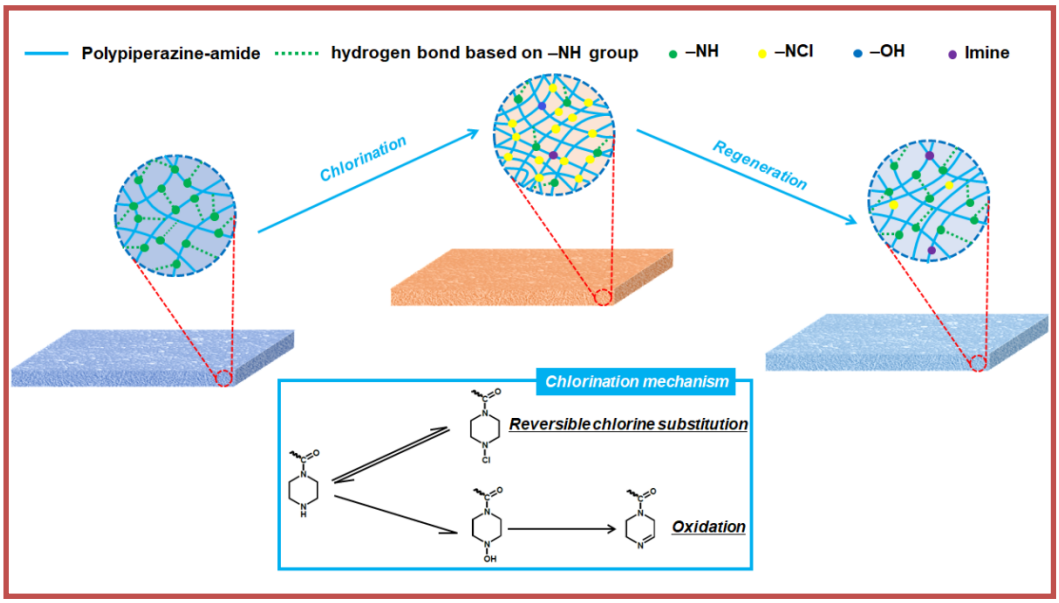

Understanding the chlorination mechanism and the chlorine-induced separation performance evolution of polypiperazine-amide nanofiltration membrane

Sihua Liu [a], Chunrui Wu [a,*], Jingguo She [a], Su Liu [b], Xiaotong Hou [a], Xiaolong Lu [a,*], Hongwei Zhang [c], Stephen Gray [d]

[a] *State Key Laboratory of Separation Membranes and Membrane Processes, Institute of Biological and Chemical Engineering, School of Material Science and Engineering, Tianjin Polytechnic University, Tianjin 300387, P. R. China. E-mail: wuchunrui@tjpu.edu.cn (C. Wu), 13920286131@163.com (X. Lu)*

[b] *School of Civil and Environmental Engineering, Georgia Institute of Technology, Atlanta, GA, 30332, United States*

[c] *State Key Laboratory of Separation Membranes and Membrane Processes, School of Environmental and Chemical Engineering, Tianjin Polytechnic University, Tianjin 300387, P. R. China*

[d] *Institute for Sustainability and Innovation, College of Engineering and Science, Victoria University, PO Box 14428, Melbourne, Victoria 8001, Australia*

Abstract

Although the tertiary amide bonds are quite stable to oxidants, the typical polypiperazine-amide (PPA) nanofiltration membranes (NFMs) were still reported to be susceptible to chlorine degradation. However, the understanding of the chlorination mechanism and the chlorine-induced separation performance evolution of the PPA NFMs still remains incomplete, significantly limiting the development of chlorine-resistant NFMs. In this work, two types of self-made PPA NFMs with different physicochemical structures and separation performance were employed to investigate

the chlorination processes. The regeneration behaviour of the chlorinated PPA NFMs was studied for the first time. Our results showed that the deterioration of the PPA separating layer upon chlorine exposure follows two pathways: reversible chlorine substitution and oxidation of the un-crosslinked -NH groups. Part of the -NCl groups could be reduced to -NH groups during the regeneration process. No cleavage of tertiary amide bonds in the PPA polymer occurred. Separation performance evolution of the PPA NFMs after chlorination or regeneration was mainly induced by the variation of -NH group content in the PPA separating layer. The loss of -NH groups after chlorination and reformation of -NH groups after regeneration could not only affect the density of the PPA separating layer through hydrogen bonds but also the electrostatic interaction between the PPA separating layer and ions. Additionally, the regenerated PPA NFMs showed good stability under elevated pressure or continuous filtration.

Keywords: Chlorination; Polypiperazine-amide; Nanofiltration membranes; Regeneration

1. Introduction

Thin-film composite (TFC) polyamide (PA) membranes fabricated through interfacial polymerization (IP) on the porous substrate are widely used for desalination and water purification [1-3]. Most commonly, fully aromatic PA separating layer formed by IP of m-phenylenediamine (MPD) and trimesoyl chloride

(TMC) is used for reverse osmosis (RO) (Fig. 1a), and semi-aromatic PA separating layer prepared by IP of piperazine (PIP) and TMC is used for nanofiltration (NF) (Fig. 1b) [4-7].

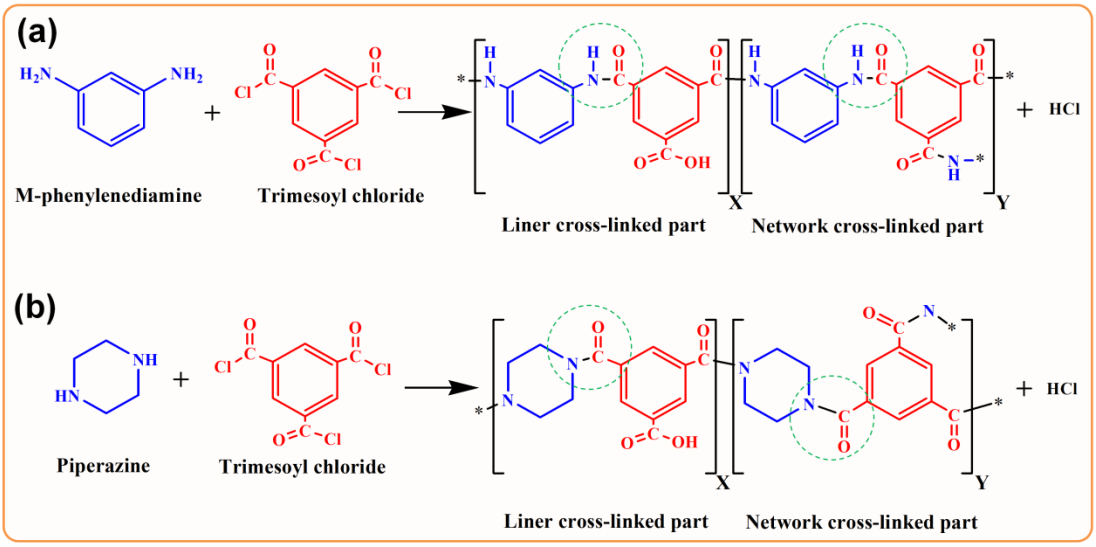

Fig. 1. IP of MPD (a) and PIP (b) with TMC, respectively.

However, the PA-based TFC membranes are sensitive to degradation by chlorine, which is commonly used as a disinfectant or membrane-cleaning agent in pre-treatment processes [8]. Understanding the chlorination mechanism and the chlorine-induced separation performance evolution of the TFC PA membranes are therefore of paramount importance in chlorine-tolerance prediction of existing membranes and designing chlorine-resistant membranes. Over the past decades, numerous studies have focused on this issue and most of them used the fully aromatic PA TFC membranes as research objects [9-10]. Currently, it is generally accepted that the deterioration of PA separating layer upon chlorine exposure follows a two-step electrophilic substitution, including a reversible N-chlorination of the amide -NH group to -NCl group, and subsequently an irreversible ring-chlorination via Orton

rearrangement [11]. Since there is no amidic hydrogen in the tertiary amides (Fig. 1b), the polypiperazine-amide (PPA) nanofiltration membranes (NFMs) were thus considered have better chlorine resistance compared with the MPD-based TFC membranes [12-13].

However, the separation performance of PPA NFMs was still reported to be damaged by chlorine exposure but previous observations and explanations appeared to be divergent [14-20]. Some studies reported a decreasing rejection and increasing water permeation after the PPA NFMs being treated with hypochlorite. This was attributed to the chlorine attack on the residual -NH groups in the PPA separating layer, or amide bond cleavage [15-16]. In other studies, the decline of water permeation accompanied with an increase or decrease of rejection was observed depending on the chlorination intensity or type of solutes. Such separation performance degradation has been attributed to the decrease in surface hydrophilicity, the change in charge property, the conformational deformation and the chain tightening [14, 17-20]. Hence, a systematic study is needed to further understand the chlorination mechanism and the chlorine-induced separation performance evolution of the PPA NFMs.

The inconsistent research results on the chlorination of PPA NFMs are presumably caused by the raw membrane materials used in the experiment. According to the previous studies, the chlorine resistance performance of PA separating layers depends strongly on their physicochemical structure, such as chemical composition and degree of network crosslinking [21]. More specifically, the separation

performance evolution of PPA NFMs after chlorine exposure was reported to be triggered by the chlorine substitution of the hydrogen atom on the un-crosslinked -NH groups in the PPA separating layers [17-18]. Most of the previous studies used the commercial membranes like NF270 (Dow-Filmtec) or self-made membranes prepared under an optimised condition to investigate the chlorination process of PPA NFMs [15-19]. The preparation conditions and modification technologies would affect the final physicochemical structure of PPA separating layers, thus possibly affect the conclusions of PPA NFMs chlorination studies.

Furthermore, the solutes employed in membrane separation performance evaluation would also affect the research results. Unlike the dense RO membranes, the separation performance, particularly the salts rejection, of the relatively loose NFMs is significantly influenced by its charge properties, which are commonly determined by the content of -NH and -COOH groups in the separating layer [22-24]. The loss of the dangling -NH groups in the PPA separating layer results in a more negatively charged separating layer which tends to exhibit higher rejection to anions and lower rejection to cations [25]. Hence, opposite trends might be observed in the change of rejection when different salts were used in the separation performance tests.

In addition, due to the reversible chlorine substitution on the -NH groups, the separation performance of the chlorinated PPA TFC membranes might be partially recovered [21]. However, to the best of our knowledge, the reversibility of the PPA NFMs chlorination process has never been investigated.

In light of the above issues, herein, two types of self-made PPA NFMs (NF-A

and NF-B) with different physicochemical structure (see part 2.2, membrane preparation) and separation performance were employed to investigate the chlorination processes of PPA NFMs. Continuous filtration experiments of the chlorinated PPA NFMs were conducted to study its regeneration behaviour. To clarify the chlorination mechanism, physicochemical structure and surface properties of the pristine membranes, chlorinated membranes, and chlorinated membranes after continuous filtration or regeneration were analysed by X-ray photoelectron spectroscopy (XPS), attenuated total reflection-fourier transform infrared spectroscopy (ATR-FTIR), zeta potential, water contact angle (WCA), field emission scanning electron microscopy (FESEM), and atomic force microscopy (AFM). To systematically elucidate the chlorine-induced membrane separation performance evolution, water flux and rejection variation to neutral solute (glucose) and four typical salts (Na_2SO_4, $MgCl_2$, $MgSO_4$, NaCl) after chlorine exposure and regeneration were determined and correlated with membrane chemical structure changes probed by the aforementioned characterization methods. The structural stability of the regenerated PPA NFMs was also evaluated.

2. Experimental section

2.1. Chemicals and Materials

Poly (vinyl chloride) (PVC) hollow fibre ultrafiltration membrane (Shenzhen Chengdelai Industry Co. Ltd., China) with a molecular weight cut-off of ~100 kDa was used as substrate. Membrane modules (Fig. S1a) were prepared according to our

previous study [26]. Anhydrous PIP (99.0 %) was purchased from Tianjin Kemiou Chemical Reagent Co. Ltd. (China) and TMC (99.0 %) was obtained from J&K Scientific Co. Ltd. (China). n-Hexane obtained from Tianjin Yingda Rare Chemical Reagents Factory (China) was used as organic phase solvent. Sodium hypochlorite (NaClO) solution with 10.0 wt.% free chlorine was procured from Tianjin Fengchuan Chemical Reagent Science And Technology Co. Ltd. (China). Other chemicals, including hydrochloric acid (HCl, ~37.0 wt.%), glucose, Na_2SO_4, $MgCl_2$, $MgSO_4$, and NaCl were obtained from Tianjin Guangfu Technology Development Co. Ltd. (China). All the chemicals were used without further purification. Deionized (DI) water was produced by a water purification system (RO50-1, Qlife, China).

2.2. Membrane preparation

As aforementioned, chlorine resistance performance of the PPA separating layer could be significantly influenced by its physicochemical structure such as -NH group content and degree of network crosslinking. To avoid the influence of physicochemical structure difference of PPA layer on the chlorination research results, two typical PPA NFMs with different physicochemical structure were prepared via manipulating the monomer concentration according to our recent work [26]. The key preparation parameters are presented in Table 1. As shown in Fig. 2, NF-B prepared under relatively high concentration ratio of PIP/TMC possesses a PPA separating layer with Janus configuration. -NH group content in the back surface (facing the substrate) of PPA separating layer of NF-B is higher than that of NF-A. As

a result, NF-B has a dually charged PPA separating layer while that of NF-A is mono-negatively charged. In addition, NF-B possesses a dense PPA separating layer with a higher degree of network crosslinking than that of NF-A (Table S1). The schematic diagram of the PPA NFMs preparation process is described in Fig. S1b, PIP aqueous solution was introduced through the lumen side of hollow fibre membrane for 5 min. Then the excess PIP solution and droplets on the membrane inner surface were removed by air sweeping. After that, the impregnated PVC support membrane module was carefully placed in TMC-hexane solution and left to stand for 2 min. The prepared membranes were dried at 25 °C for 15 min and then rinsed with and preserved in DI water.

Table 1 Key preparation parameters of the NFMs used in this work.

Membranes	PIP concentration (%)	TMC concentration (%)	Reaction time (s)	Organic phase temperature (°C)
NF-A	0.3	0.3	120	0
NF-B	1.0	0.1	120	0

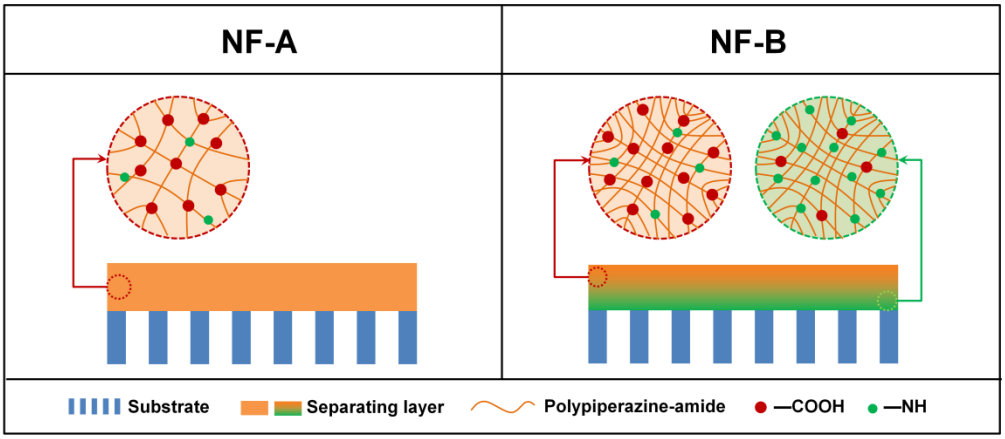

Fig. 2. Configurations of NF-A and NF-B.

2.3. Membrane chlorination and regeneration

The chlorination was performed by soaking the membrane modules (rinsed by DI water before) in NaClO solutions (25±1 °C) for 1 hour. An extremely high NaClO concentration of 2000 $mg \cdot L^{-1}$ was chosen to accelerate the degradation process in the laboratory. Since the PPA NFMs are commonly used in a neutral circumstance, the NaClO solutions were adjusted to pH=7 with HCl and NaOH. Samples after chlorination were rinsed by DI water to remove the absorbed chlorine prior to further treatments or measurements.

In order to investigate the regeneration behaviour of the chlorinated PPA NFMs, continuous filtration experiments were performed. Water flux and rejection were measured and normalized by the initial value at certain time intervals until the water flux reached a steady state. It is worth noting that regenerated membrane samples for characterization were all prepared upon continuous filtration with DI water for 5 hours under an operation pressure of 0.35 MPa.

2.4. Membrane characterization

ATR-FTIR and XPS analysis were carried out to study the chemical information changes after chlorination and regeneration. The XPS (K-alpha, Thermo Fisher, USA) measurements were performed on a Quanta 200 spectrometer using monochromatized Al Kα radiation at 1486.6 eV. ATR-FTIR spectra were collected using a Vector-22 spectrometer (Nicolet iS50, Thermo Fisher, USA) with Zinc Selenide (ZnSe) as an internal reflection element at an incident angle of 45°. Each spectrum was collected

by the accumulation of 16 scans at a resolution of 4 cm^{-1}. It should be noted that the ATR-FITR analyses in previous studies were performed on the composite membranes rather than the PPA separating layers [27-28]. To clearly determine the variation of -NH groups and hydrogen bonds in the PPA polymer after chlorination and regeneration, free-standing PPA films were prepared by IP at the bulk liquid surface and used to conduct the ATR-FTIR measurements. Detailed preparation and treatment processes of the samples were described in the supplementary material (Fig. S2).

Charge properties of samples were detected using an electrokinetic analyser (SurPASS, Anton Paar, Austria) [24]. Fibres were immobilized in a module in advance to analyse the charge properties of membrane inner surface. WCA was measured by a contact angle instrument (SPCA, Hake Test Instrument, China) at room temperature. DI water droplets (about 5.0 μL) were deposited on the membrane surface and the images were captured 3 seconds later. For the measurement, at least five parallel membrane samples were selected, and five random locations were tested for each sample to get a reliable value. Morphologies and roughness of membrane surface were observed and analysed via FESEM (Gemini SEM500, ZEISS, Germany) and AFM (Agilent, S5500, USA), respectively. All hollow fibre samples were cut open and then flattened before the two measurements. The samples were sputter-coated with gold prior to the FESEM observation.

2.5. Separation performance test

Separation performance of the hollow fibre NFMs was evaluated using a cross-

flow nanofiltration system (Fig. S3). All water flux and rejection data were obtained under 0.35 MPa at 25 °C. The water flux (F, L·m^{-2}·h^{-1}) was calculated as follows:

$$F = \frac{V}{A \cdot t} \quad (1)$$

where V, A, and t are the volume of permeated water (L), the valid membrane filtration area (m^2), and the permeation time (h), respectively. Solute rejection (R, %) was calculated by using the following equation:

$$R = \left(1 - \frac{C_p}{C_f}\right) \times 100\,\% \quad (2)$$

where C_f and C_p (mg·L^{-1}) are the solute concentration of the feed and permeate solution, respectively. The concentration of electrolyte and neutral organic solute were measured with a conductivity meter (DDS-11A, Rex, China) and TOC analyzer (TOC-VCSH, Shimadzu, Japan), respectively.

3. Results and discussion

3.1. Chemical structure changes of PPA NFMs after chlorination and regeneration

Changes in chemical composition and bonding at the surfaces of the two selected PPA NFMs aroused by chlorination and regeneration were studied by XPS (Table 2). Newly uptake of chlorine after chlorination and apparent dechlorination after regeneration were observed for both two selected NFMs. The Cl/N ratio of the two chlorinated membranes was much less than 1, which was consistent with previous reports [17-18]. The small amount of incorporated chlorine should be attributed to the chlorine substitution of the un-crosslinked -NH groups in the PPA separating layer to -NCl groups. Dechlorination after regeneration is ascribed to that some -NCl groups

were reduced to -NH groups [21]. As aforementioned, NF-B membrane prepared under relatively high PIP concentration and low TMC concentration possesses a PPA separating layer with a higher content of -NH groups [26], which was supposed to be more vulnerable to chlorine attack. Interestingly, however, the amount of incorporated chlorine to the NF-B membrane was slightly smaller than that of NF-A membrane. This is due to that high levels of crosslinking improve the chlorine resistance (Table S1) [12].

Table 2 chemical composition changes of the surfaces of the two selected NFMs aroused by chlorination and regeneration.

Membranes	Atomic composition (%)				O/N	O/C
	C	N	O	Cl		
NF-A (Pristine)	73.60	9.70	16.70	0.00	1.72	0.23
NF-A (After chlorination)	69.90	10.20	17.70	2.20	1.73	0.25
NF-A (After regeneration)	71.80	10.20	17.30	0.70	1.70	0.24
NF-B (Pristine)	73.60	10.90	15.50	0.00	1.42	0.21
NF-B (After chlorination)	70.40	9.50	18.30	1.80	1.93	0.26
NF-B (After regeneration)	72.00	10.00	17.20	0.80	1.72	0.24

In addition to chlorine content variation, the content of oxygen, O/N and O/C ratio increased after chlorination. Moreover, the oxygen content, O/N and O/C ratio exhibited distinct tendency of recovery after regeneration. For the polyamide layer, the increase of O/N ratio is commonly ascribed to the decrease of degree of network crosslinking. However, the tertiary amide bonds of the PPA layer are quite stable at

neutral pH levels [12]. Even if the amide bonds were hydrolysed to carboxyl and amine groups, polymerization reaction between these two groups is unlikely to occur in the ambient temperature DI water [29]. Hence, the amide bond cleavage is not a plausible mechanism to explain the oxygen content changes [18].

A possible mechanism accounting for the variation of oxygen content was described as follows (Fig. 3). Based on the oxidation mechanism of organic amine, the secondary amine would be oxidized to hydroxylamine, which increased the oxygen content in the PPA separating layer [30]. However, the hydroxylamine is unstable and tends to lose water to form imine-like species leading to the decrease of oxygen content [12, 31-32]. It should be noted that the oxidation would result in the cleavage of secondary amine linkages but not the tertiary amide bonds.

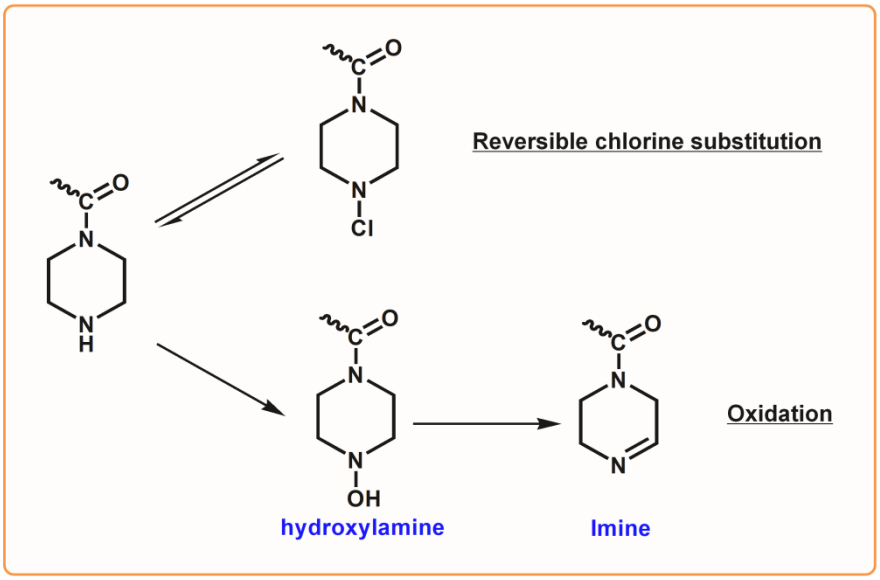

Fig. 3. Possible chlorination mechanism of PPA NFMs.

The bulk chemistry changes occurring in the PPA polymer after chlorination and regeneration were studied via ATR-FTIR using the free-standing PPA film as analysis object. As shown in Fig. 4, the band intensity at 1608 cm^{-1} and 3390 cm^{-1} representing

the hydrogen-bonded C=O and -NH stretching [21], respectively, decreased after chlorination and partially recovered after regeneration. This result suggests that hydrogen bonds between -NH and C=O were damaged or weakened resulting from the chlorine substitution and oxidation of the un-crosslinked -NH groups after chlorination. Due to the reversibility of the chlorine substitution, part of the -NCl groups could be reduced to -NH groups and thus the -NH groups based hydrogen bonds would be partially reformed after regeneration.

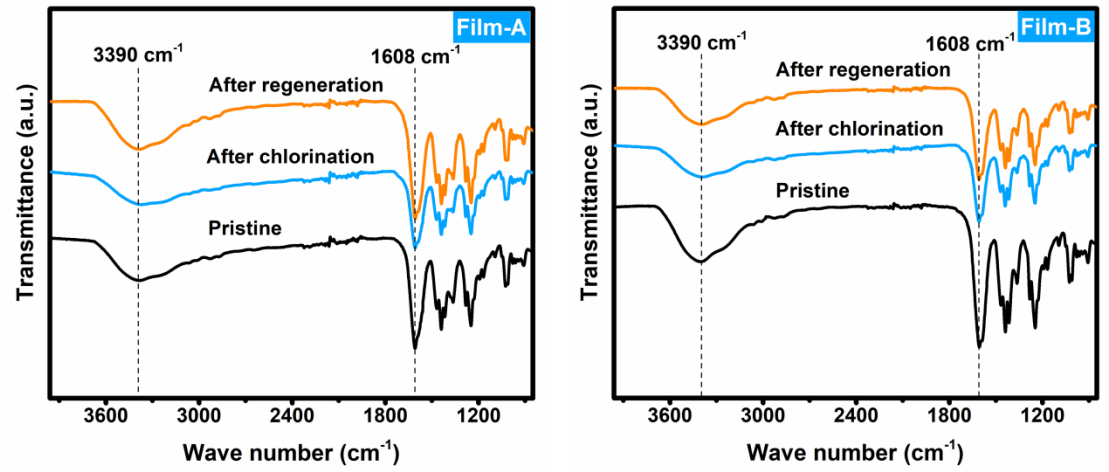

Fig. 4. ATR-FTIR spectra of Film-A and Film-B after chlorination and regeneration. The preparation parameters and treatment processes of Film-A and Film-B (Fig. S2) are similar to that of NF-A and NF-B, respectively. It was believed that the free-standing PPA film had similar physicochemical structure to the PPA separating layer prepared on support membrane.

3.2. Changes in NFMs surface charge property

The surface charge of NF-A and NF-B membranes before and after chlorination and regeneration is presented in Fig. 5. Both the NF-A and NF-B became more negatively charged after chlorination, which could be attributed to the decrease of -NH group content caused by chlorine substitution and oxidation of the un-crosslinked -NH groups [21]. After regeneration, however, both the two membranes became more

positively charged at high pH value, which could be attributed to the reduction of -NCl groups to -NH groups as described in Fig. 3. It is worth noting that zeta potential variation magnitudes with pH of the two regenerated membranes are different from that of pristine and chlorinated ones. This phenomenon might be ascribed to the formation of imine species after regeneration.

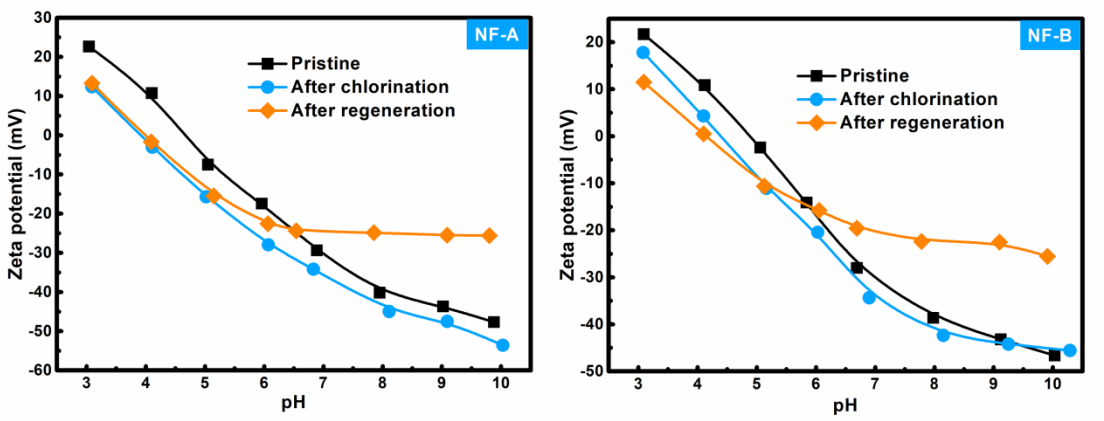

Fig. 5. Zeta potential for pristine, chlorinated and regenerated PPA NFMs as a function of pH.

3.3. Surface morphology changes of PPA NFMs after chlorination and regeneration

Surface morphology of the pristine, chlorinated and regenerated PPA NFMs was examined by FESEM, as shown in Fig. 6. No physical damage like cracks or ruptures presented on the surfaces of chlorinated and regenerated PPA NFMs, further confirming that the tertiary amide bonds of PPA are quite stable upon chlorine exposure. However, notable morphology changes after chlorination and regeneration could be observed from the SEM images. For the NF-A membrane, wrinkled morphology appeared after chlorination and the wrinkles disappeared after regeneration. The chlorine-induced morphology changes might be explained by the

enhanced ductility of the PPA separating layer after chlorination due to the breakage of hydrogen bonds between polymer chains as confirmed by the ATR-FTIR measurement (Fig. 4) [18, 33-34]. After regeneration, some of the -NCl groups were reduced to -NH groups and thus new hydrogen bonds formed leading to the morphology recover. For the NF-B membranes, however, there are no observable wrinkled morphologies after chlorination which could be attributed to its dense PPA separating layer with a higher degree of network crosslinking (Table S1) [12].

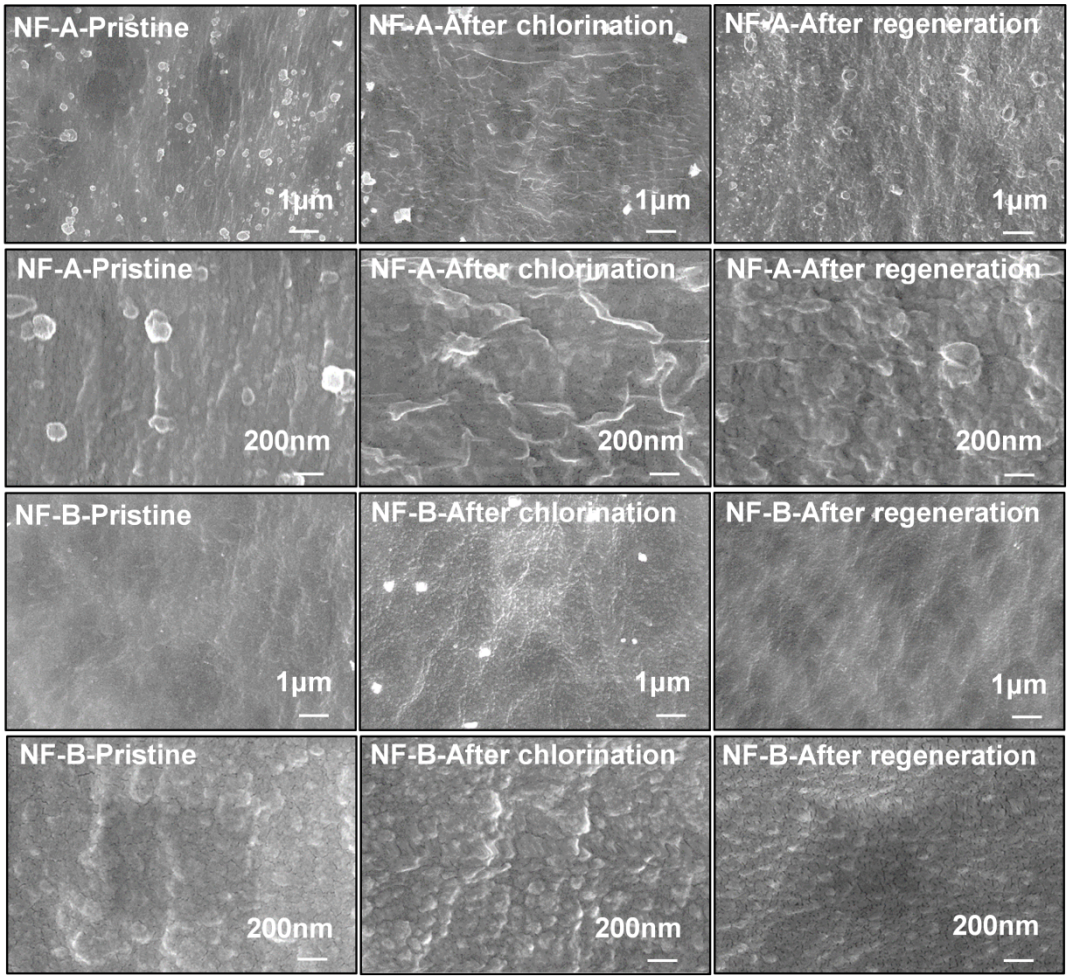

Fig. 6. Top down SEM images of NFMs.

3.4. Changes in NFMs surface wettability

WCA data presented in Table 3 shows that WCA of both the two NFMs decreased after chlorination and recovered after regeneration. The chlorine substitution process incorporated chlorine into the membrane surface which should lead to a more hydrophobic surface [35]. However, since hydroxyl group is more hydrophilic than amine groups due to its stronger electronegativity, the oxidation of secondary amine to hydroxylamine would increase the hydrophilicity of membrane surface [36]. In addition, according to the Wenzel model, for a hydrophilic surface, the hydrophilicity will be enhanced by the increased surface roughness (Fig. 6 and Fig. S5) [37]. After regeneration, the dechlorination and morphology recovery will lead to the recovery of surface wettability. Hence, the variation of wettability could be explicated by the competing effects of oxidation and reversible chlorine substitution of the -NH groups, and the induced surface roughness change.

Overall, changes of membrane surface physicochemical structure and property after chlorination and regeneration are well consistent with the proposed chlorination mechanism described in Fig. 3.

Table 3 Water contact angle for pristine, chlorinated and regenerated PPA NFMs.

WCA (°)	Pristine	After chlorination	After regeneration
NF-A	27.6±1.3	22.6±2.4	25.1±1.1
NF-B	48.7±2.8	36.6±3.5	53.0±3.9

3.5. Separation performance evolution

Separation performance of the two pristine NFMs towards salts and neutral solute were evaluated, as shown in Table 4. The salts rejection order of NF-A membrane is Na_2SO_4 > $MgSO_4$ > $MgCl_2$ > NaCl, which indicates that the NFM surface is mono-negatively charged. In sharp contrast, The NF-B membrane exhibits a different salts rejection order of $MgSO_4$ > $MgCl_2$ > Na_2SO_4 > NaCl, which reveals that the PPA separating layer of this NFM is dually charged with a negatively charged top surface and a positively charged back (facing the substrate) surface [24, 26]. In addition, compared with NF-A membrane, the NF-B membrane shows higher rejection to glucose indicates that its PPA layer has a smaller pore size than that of NF-A membrane [38].

Table 4 Original separation performance of the two selected NFMs in this work.

Solutes	*R* (%)		*F* ($L \cdot m^{-2} \cdot h^{-1}$)	
	NF-A	NF-B	NF-A	NF-B
Na_2SO_4	95.4±0.9	89.4±1.9	50.4±1.1	38.5±0.3
$MgCl_2$	25.0±1.8	97.8±0.8	56.9±1.2	40.7±3.2
$MgSO_4$	91.4±1.9	99.0±0.5	57.5±0.5	42.1±1.8
NaCl	20.5±0.7	60.7±3.1	61.1±1.0	48.7±2.7
Glucose	67.9±2.0	84.6±2.5	57.5±1.5	45.5±1.2

Test conditions: Glucose concentration = 200 $mg \cdot L^{-1}$, divalent salts concentration = 1000 $mg \cdot L^{-1}$, NaCl concentration = 500 $mg \cdot L^{-1}$, 25 °C, 0.35 MPa.

After chlorination and regeneration, a series of interesting phenomena about

separation performance variation were observed. Change rate of rejection after regeneration were employed to demonstrate the rejection performance variation induced by chlorination and regeneration, as shown in Fig. 7.

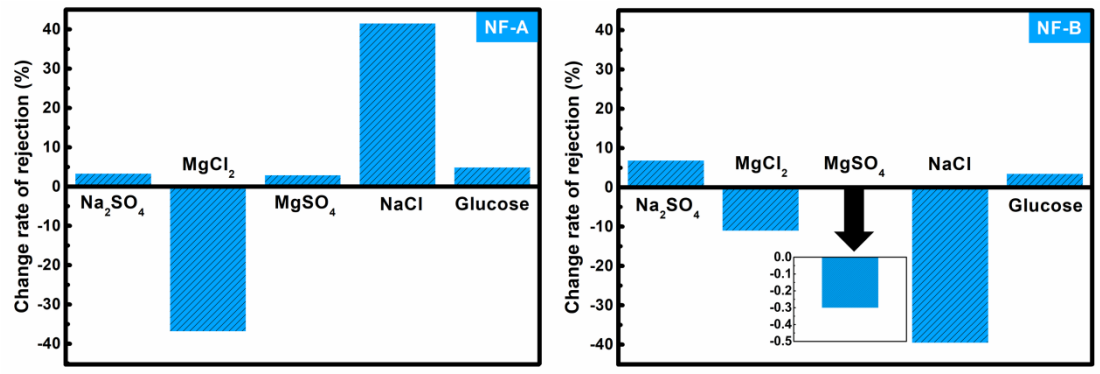

Fig. 7. Change rate of rejections of the selected PPA NFMs after chlorination and regeneration.

From Fig. 7 we can see, rejections to Na_2SO_4 and glucose increased while rejections to $MgCl_2$ decreased for both the two PPA NFMs after chlorination and regeneration. This phenomenon can be explained as follows: after chlorination, content of -NH groups in the PPA separating layer decreased and thus the hydrogen bonds based on the -NH groups destroyed (Fig. 4) leading to the structural compression of the PPA chain network under relatively high pressure, which could be confirmed by the increased glucose rejection. In addition, the decrease of -NH group content would weaken the electrostatic repulsion effect between the PPA separating layer and cations leading to the decrease of $MgCl_2$ rejection, although the PPA separating layer became denser. Meanwhile, the decrease of -NH group content would also weaken the electrostatic attraction effect between the PPA layer and anions, thus contributing to the increase of Na_2SO_4 rejection [39-40]. It is worth noting that

proceeding proper chlorination treatment to the PPA NFMs might be a facile method to improve both the divalent anions rejection and the separation ratio of divalent anions to cations.

More interestingly, there are some different separation performance changes between NF-A and NF-B membranes. The rejection order of NF-B membrane after chlorination changed to $MgSO_4$ > Na_2SO_4 > $MgCl_2$ > NaCl which could be attributed to that the dually charged PPA separating layer of NF-B became mono-negatively charged after chlorination [24]. Additionally, rejection of NF-A membrane to $MgSO_4$ and NaCl increased after chlorination and regeneration while that of NF-B decreased. As aforementioned, the chlorinated PPA separating layers of both the two membranes are easy to be compressed, which would enhance the size sieving effect and lead to the increase of solutes rejection. However, the electrostatic repulsion between cations and -NH groups in the PPA separating layer plays a crucial role in cations rejection of NF-B membrane [26]. Hence, the disappearance of the -NH groups would decrease the rejection of NF-B membrane to cations especially to the monovalent cations with small hydrated ionic radius like Na^+.

Next, we investigated the separation performance evolution during the regeneration process of the chlorinated PPA NFMs. To identify the variation of separation mechanism of the chlorinated PPA NFMs including electrostatic interaction and size sieving during the regeneration process, water flux and solutes rejection (Na_2SO_4, $MgSO_4$, $MgCl_2$, NaCl and glucose) of chlorinated NF-A and NF-B membranes were measured and normalized by the initial value at certain time

intervals. As shown in Fig. 8, water flux of both NF-A and NF-B membranes decreased after chlorination which should be attributed to the compression of PPA layer as described above. During the regeneration process, water flux of the two chlorinated PPA NFMs increased with increasing operation time and finally reached a stable value, while the variation of solutes rejection with operation time strongly depended on the types of membranes and solutes. The rejections of chlorinated NFMs to glucose are higher than that of pristine membranes indicates that the chlorinated NFMs possess denser separating layers. The glucose rejection of the chlorinated NFMs showed an overall decrease trend during the regeneration processes with increasing operation time until reaching stable values which are still higher than that of pristine membranes. This result indicates that the chlorinated PPA separating layer would recover loose step by step until reaching a stable state which still denser than the pristine one, further confirming that the hydrogen bonds between polymer chains could be partially reformed during the regeneration process. Meanwhile, as aforementioned, the reduction of -NCl groups to -NH groups would also affect the electrostatic interactions between ions and the PPA separating layer and thus affect the rejection to salts. Rejection to $MgCl_2$ and $MgSO_4$ of both the chlorinated NF-A and NF-B membranes increased gradually during the regeneration process due to the increasing electrostatic repulsion between Mg^{2+} and the PPA separating layer. For the salt of NaCl, rejection of both the membranes decreased during the regeneration process, which should be attributed to the recovery of conformation based on the -NH groups. Interestingly, rejection to Na_2SO_4 of both the two membranes almost

unchanged during the regeneration process, which could ascribe to the relatively large hydrated radius of SO_4^{2-} [41]. In summary, the evolution of salts rejection of the chlorinated PPA NFMs during the regeneration process should be attributed to the variation of separation mechanism including the electrostatic interaction and size sieving effect, which is induced by the regeneration of -NH groups.

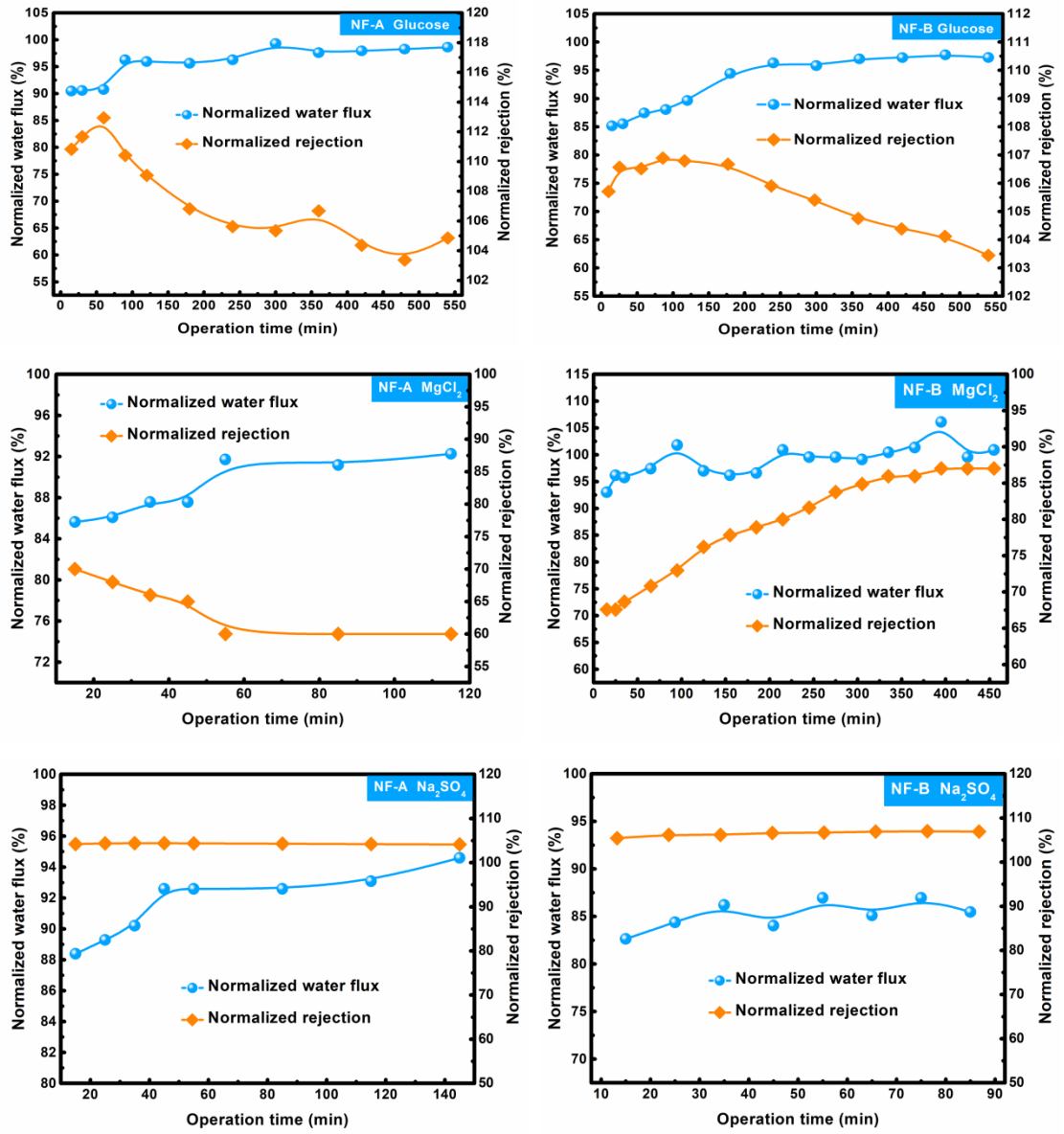

Fig. 8. Water flux and solutes rejection of the two chlorinated PPA NFMs varied with operation time. Test conditions: Glucose concentration = 200 mg·L^{-1}, divalent salts concentration = 1000 mg·L^{-1}, NaCl concentration = 500 mg·L^{-1}, 25 °C, 0.35 MPa.

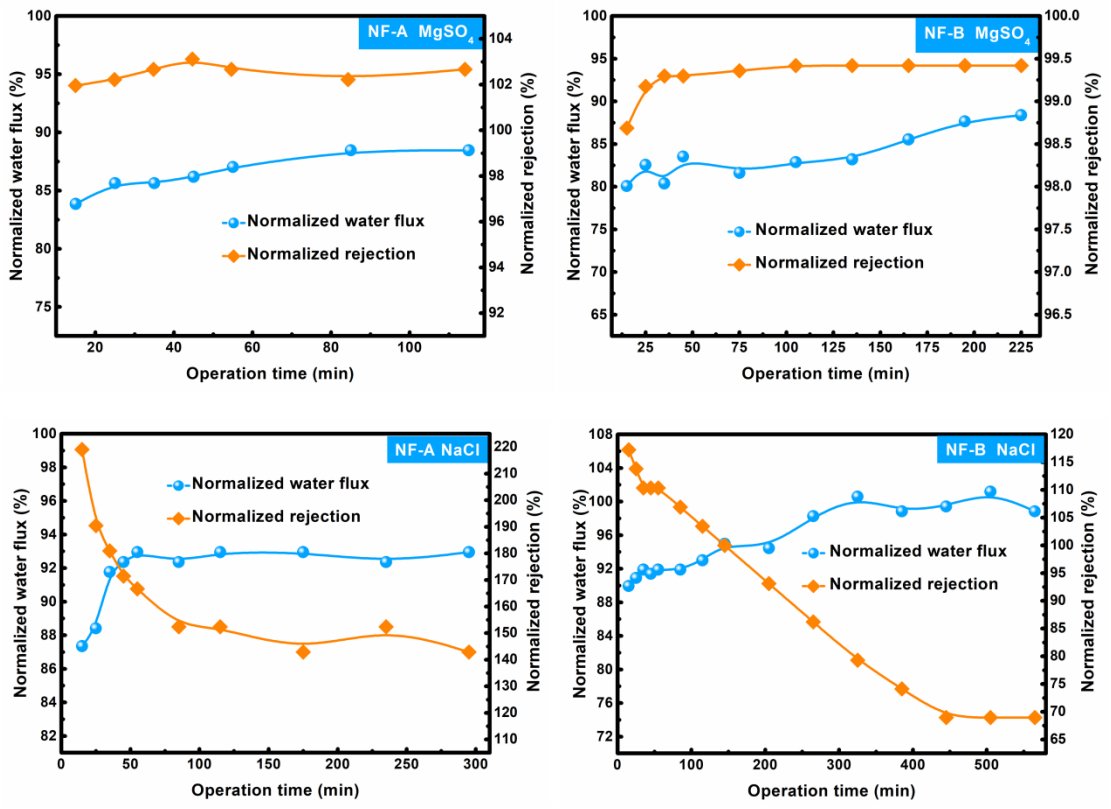

Fig. 8. (*continued*).

3.6. Structural stability evaluation of the regenerated PPA NFMs

The structural stability of the regenerated PPA NFMs was evaluated by examining its separation performance variation under improved operation pressure and continuous filtration. As shown in Fig. 9, water flux of the regenerated NF-A and NF-B increased proportionally with increasing the operating pressure and the Na_2SO_4 rejection also increased slightly. In the continuous filtration experiments, no obvious change of water flux and salt rejection was observed. These results indicate that both the two regenerated PPA NFMs possess good structural stability [42].

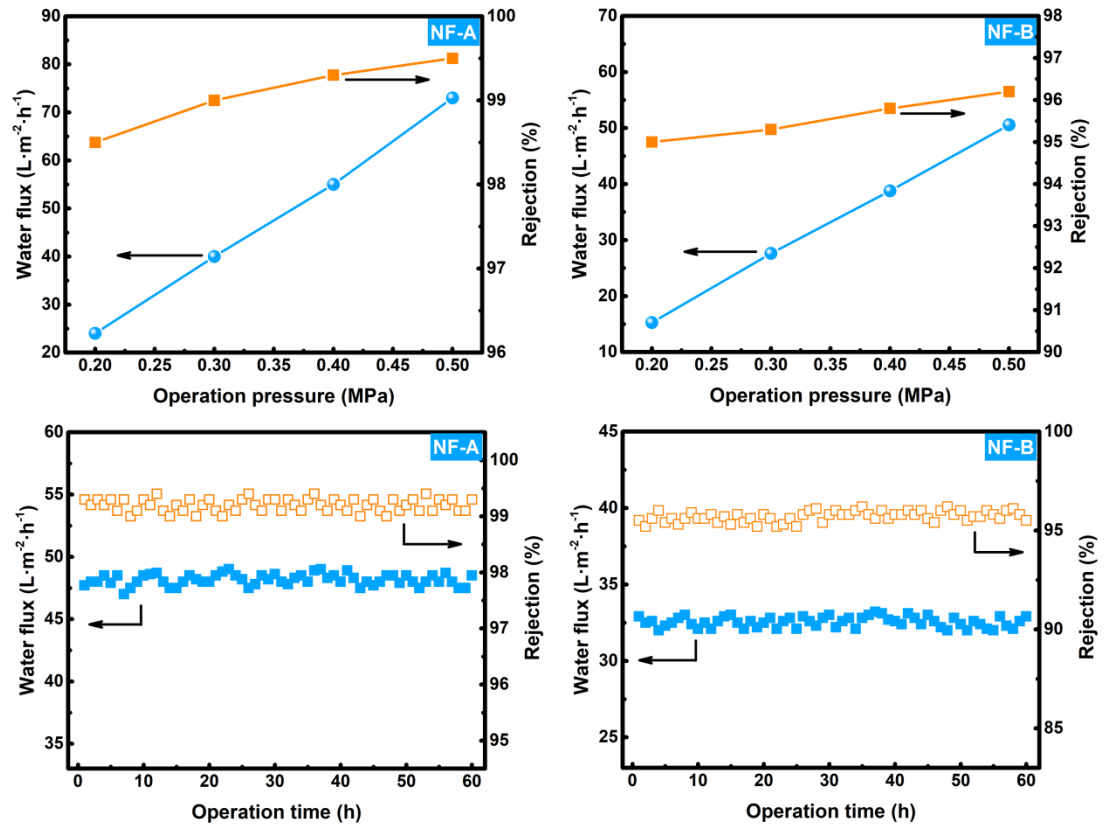

Fig. 9. Structural stability evaluation of the regenerated NF-A and NF-B. Test conditions: Na_2SO_4 concentration = 1000 mg·L^{-1}, 25 °C, 0.35 MPa.

4. Conclusions

Two types of self-made PPA NFMs with different chemical composition, degree of network crosslinking, and separation performance were employed to investigate the chlorination mechanism and the chlorine-induced separation performance evolution of the PPA NFMs. The regeneration process of the chlorinated PPA NFMs was investigated for the first time. The data presented in this study suggest that the deterioration of PPA separating layer upon chlorine exposure mainly follows two pathways: reversible chlorine substitution and oxidation of the un-crosslinked -NH groups. Part of the -NCl groups could be reduced to -NH groups during the

regeneration process. No cleavage of tertiary amide bonds of the PPA polymer was observed in our study. Water flux of both the two PPA NFMs decreased after chlorination and partially recovered after regeneration, while rejection performance evolution depended on the types of NFMs and solutes, which was attributed to the following two reasons: 1) Hydrogen bonds based on -NH groups destroyed after chlorination and partially reformed after regeneration, resulting in ductility variation of the PPA separating layer, which affected the density or steric hindrance of the separating layer under pressure; 2) Variation of -NH group content in the PPA separating layer after chlorination or regeneration would affect the electrostatic repulsion effect between the PPA separating layer and cations and the electrostatic attraction effect between the PPA layer and anions. The findings in this work could possibly explicate the inconsistent research results on PPA NFMs chlorination reported in the literature.

Acknowledgements

This study was supported by National Natural Science Foundation of China (51638011, 51578376), the Program for Innovative Research Team in University of Tianjin (No. TD13-5044), the Research Program of Application Foundation and Advanced Technology, Tianjin, China (13JCQNJC08800), and Key Projects in the Tianjin Science & Technology Pillar Program (15ZCZDSF00070).

Appendix A. Supplementary material

Supplementary data to this article can be found online or obtained from the author.

References

[1] A. G. Fane, R. Wang, M. X. Hu, Synthetic membranes for water purification: status and future, Angew. Chem. Int. Ed. 54 (2015) 3368-3386.

[2] M. J. T. Raaijmakers, N. E. Benes, Current trends in interfacial polymerization chemistry, Prog. Polym. Sci. 63 (2016) 86-142.

[3] Y.-L. Ji, Q.-F. An, X.-D. Weng, W.-S. Hung, K.-R. Lee, C.-J. Gao, Microstructure and performance of zwitterionic polymeric nanoparticle/polyamide thin-film nanocomposite membranes for salts/organics separation, J. Membr. Sci. 548 (2018) 559-571.

[4] J. R. Werber, C. O. Osuji, M. Elimelech, Materials for next-generation desalination and water purification membranes, Nat. Rev. Mater. 1 (2016) 16018-16032.

[5] Z. Tan, S. Chen, X. Peng, L. Zhang, C. Gao, Polyamide membranes with nanoscale Turing structures for water purification, Science 360 (2018) 518-521.

[6] Q. An, F. Li, Y. Ji, H. Chen, Influence of polyvinyl alcohol on the surface morphology, separation and anti-fouling performance of the composite polyamide nanofiltration membranes, J. Membr. Sci. 367 (2011) 158-165.

[7] D. Hu, Z.-L. Xu, C. Chen, Polypiperazine-amide nanofiltration membrane containing silica nanoparticles prepared by interfacial polymerization, Desalination 301 (2012) 75-81.

[8] K. L. Cho, A. J. Hill, F. Caruso, S. E. Kentish, Chlorine resistant glutaraldehyde crosslinked polyelectrolyte multilayer membranes for desalination, Adv. Mater. 27 (2015) 2791-2796.

[9] R. Verbeke, V. Gómez, I. F. J. Vankelecom, Chlorine-resistance of reverse osmosis (RO) polyamide membrane, Prog. Polym. Sci. 72 (2017) 1-15.

[10] N. P. Soice, A. C. Maladono, D. Y. Takigawa, A. D. Norman, W. B. Krantz, A. R. Greenberg, Oxidative degradation of polyamide reverse osmosis membranes: studies of molecular model compounds and selected membranes, J. Appl. Polym. Sci. 90 (2003) 1173-1184.

[11] H. Huang, S. Lin, L. Zhang, L. Hou, Chlorine-resistant polyamide reverse osmosis membrane with monitorable and regenerative sacrificial layers, ACS Appl. Mater. Interfaces 9 (2017) 10214-10223.

[12] J. Glater, S.-K. Hong, M. Elimelech, The search for a chlorine-resistant reverse osmosis membrane, Desalination 95 (1994) 325-345.

[13] D. Wu, J. Martin, J. R. Du, Y. Zhang, D. Lawless, X. Feng, Effects of chlorine exposure on nanofiltration performance of polyamide membranes, J. Membr. Sci. 487 (2015) 256-270.

[14] A. Simon, L. D. Nghiem, P. Le-Clech, S. J. Khan, J. E. Drewes, Effects of membrane degradation on the removal of pharmaceutically active compounds (PhACs) by NF/RO filtration processes, J. Membr. Sci. 340 (2009) 16-25.

[15] Y Zhu, W. Xie, S. Gao, F. Zhang, W. Zhang, Z. Liu, J. Jin, Single-walled carbon nanotube film supported nanofiltration membrane with a nearly 10 nm thick polyamide selective layer for high-flux and high-rejection desalination, Small 12 (2016) 5034-5041.

[16] S.-M. Xue, C.-H. Ji, Z.-L. Xu, Y.-J. Tang, R.-H. Li, Chlorine resistant TFN nanofiltration membrane incorporated with octadecylamine-grafted GO and fluorine-containing monomer, J. Membr. Sci. 545 (2018) 185-195.

[17] V. T. Do, C. Y. Tang, M. Reinhard, J. O. Leckie, Degradation of polyamide nanofiltration

and reverse osmosis membranes by hypochlorite, Environ. Sci. Technol. 46 (2012) 852-859.

[18] J.-H. Lee, J. Y. Chung, E. P. Chan, C. M. Stafford, Correlating chlorine-induced changes in mechanical properties to performance in polyamide-based thin film composite membranes, J. Membr. Sci. 433 (2013) 72-79.

[19] Y.-J. Tang, Z.-L. Xu, S.-M. Xue, Y.-M. Wei, H. Yang, Improving the chlorine-tolerant ability of polypiperazine-amide nanofiltration membrane by adding NH_2-PEG-NH_2 in the aqueous phase, J. Membr. Sci. 538 (2017) 9-17.

[20] V. T. Do, C. Y. Tang, M. Reinhard, J. O. Leckie, Effects of hypochlorous acid exposure on the rejection of salt, polyethylene glycols, boron and arsenic (V) by nanofiltration and reverse osmosis membranes, Water Res. 46 (2012) 5217-5223.

[21] J. Xu, Z. Wang, X. Wei, S. Yang, J. Wang, S. Wang, The chlorination process of crosslinked aromatic polyamide reverse osmosis membrane: New insights from the study of self-made membrane, Desalination 313 (2013) 145-155.

[22] X. Yang, Y. Du, X. Zhang, A. He, Z.-K. Xu, Nanofiltration membrane with a mussel-inspired interlayer for improved permeation performance, Langmuir 33 (2017) 2318-2324.

[23] W. Fang, L. Shi, R. Wang, Interfacially polymerized composite nanofiltration hollow fiber membranes for low-pressure water softening, J. Membr. Sci. 430 (2013) 129-139.

[24] C. Wu, S. Liu, Z. Wang, J. Zhang, X. Wang, X. Lu, Y. Jia, W.-S. Hung, K.-R. Lee, Nanofiltration membranes with dually charged composite layer exhibiting super-high multivalent-salt rejection, J. Membr. Sci. 517 (2016) 64-72.

[25] H. Wang, Q. Zhang, S. Zhang, Positively charged nanofiltration membrane formed by interfacial polymerization of 3,3',5,5'-biphenyl tetraacyl chloride and piperazine on a

poly(acrylonitrile) (PAN) support, J. Membr. Sci. 378 (2011) 243-249.

[26] S. Liu, C. Wu, W.-S. Hung, X. Lu, K.-R. Lee, One-step constructed ultrathin Janus polyamide nanofilms with opposite charges for highly efficient nanofiltration, J. Mater. Chem. A 5 (2017) 22988-22996.

[27] Z. Zhang, Z. Wang, J. Wang, S. Wang, Enhancing chlorine resistances and anti-biofouling properties of commercial aromatic polyamide reverse osmosis membranes by grafting 3-allyl-5,5-dimethylhydantoin and N,N'-Methylenebis (acrylamide), Desalination 309 (2013) 187-196.

[28] R. Verbeke, V. Gómez, T. Koschine, S. Eyley, A. Szymczyk, M. Dickmann, T. Stimpel-Lindner, W. Egger, W. Thielemans, I. F. J. Vankelecom, Real-scale chlorination at pH4 of BW30 TFC membranes and their physicochemical characterization, J. Membr. Sci. 551 (2018) 123-135.

[29] J. Peng, Y. Su, W. Chen, X. Zhao, Z. Jiang, Y. Dong, Y. Zhang, J. Liu, X. Cao, Polyamide nanofiltration membrane with high separation performance prepared by EDC/NHS mediated interfacial polymerization, J. Membr. Sci. 427 (2013) 92-100.

[30] N. Greeves, S. Warren, P. Wothers, J. Clayden, Organic chemistry, Oxford University Press, USA, 2000, pp. 1357.

[31] G.-D. Kang, C.-J. Gao, W.-D. Chen, X.-M. Jie, Y.-M. Cao, Q. Yuan, Study on hypochlorite degradation of aromatic polyamide reverse osmosis membrane, J. Membr. Sci. 300 (2007) 165-171.

[32] H.-Z. Zhang, Z.-L. Xu, Y.-J. Tang, H. Ding, Highly chlorine-tolerant performance of three-channel capillary nanofiltration membrane with inner skin layer, J. Membr. Sci. 527 (2017) 111-120.

[33] Y.-N. Kwon, J. O. Leckie, Hypochlorite degradation of crosslinked polyamide membranes II.

Changes in hydrogen bonding behavior and performance, J. Membr. Sci. 282 (2006) 456-464.

[34] W. Guo, C. M. Reese, L. Xiong, P. K. Logan, B. J. Thompson, C. M. Stafford, A. V. Ievlev, B. S. Lokitz, O. S. Ovchinnikova, D. L. Patton, Buckling instabilities in polymer brush surfaces via postpolymerization modification, Macromolecules 50 (2017) 8670-8677.

[35] J. M. Gohil, A. K. Suresh, Chlorine attack on reverse osmosis membranes: Mechanisms and mitigation strategies, J. Membr. Sci. 541 (2017) 108-126.

[36] S.-M. Xue, Z.-L. Xu, Y.-J. Tang, C.-H. Ji, Polypiperazine-amide nanofiltration membrane modified by different functionalized multiwalled carbon nanotubes (MWCNTs), ACS Appl. Mater. Interfaces 8 (2016) 19135-19144.

[37] M. Tao, L. Xue, F. Liu, L. Jiang, An intelligent superwetting PVDF membrane showing switchable transport performance for oil/water separation, Adv. Mater. 26 (2014) 2943-2948.

[38] C. Liu, L. Shi, R. Wang, Crosslinked layer-by-layer polyelectrolyte nanofiltration hollow fiber membrane for low-pressure water softening with the presence of SO_4^{2-} in feed water, J. Membr. Sci. 486 (2015) 169-176.

[39] W. Fang, L. Shi, R. Wang, Mixed polyamide-based composite nanofiltration hollow fiber membranes with improved low-pressure water softening capability, J. Membr. Sci. 468 (2014) 52-61.

[40] Z. Wang, K. Xiao, X.-M. Wang, Role of coexistence of negative and positive membrane surface charges in electrostatic effect for salt rejection by nanofiltration, Desalination 443 (2018) 245-255.

[41] Y. Du, Y. Lv, W.-Z. Qiu, J. Wu, Z.-K. Xu, Nanofiltration membranes with narrowed pore size distribution via pore wall modification, Chem. Commun. 52 (2016) 8589-8592.

[42] X. Li, C. Zhang, S. Zhang, J. Li, B. He, Z. Cui, Preparation and characterization of positively charged polyamide composite nanofiltration hollow fiber membrane for lithium and magnesium separation, Desalination 369 (2015) 26-36.

Figures

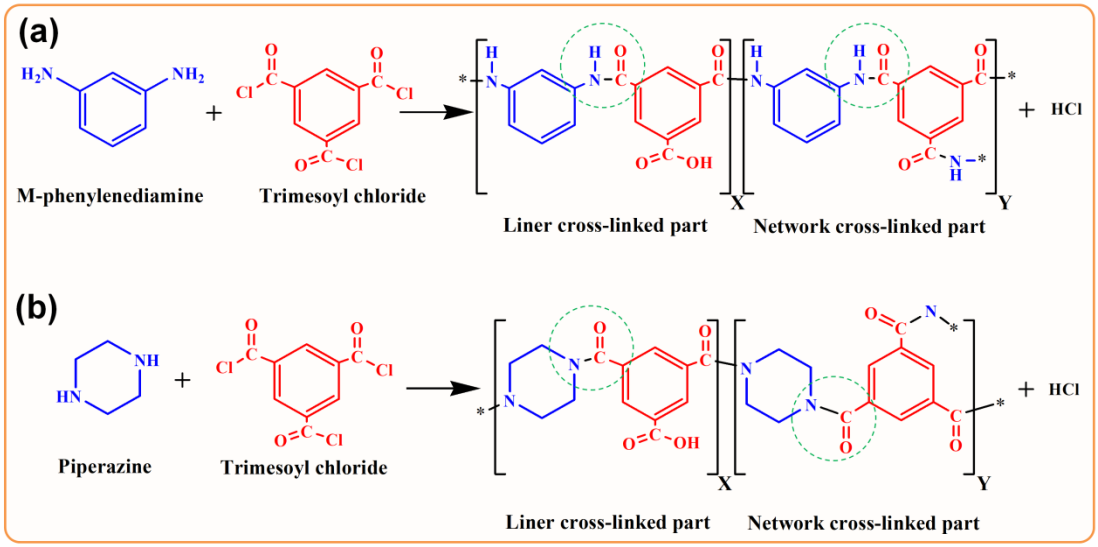

Fig. 1. IP of MPD (a) and PIP (b) with TMC, respectively.

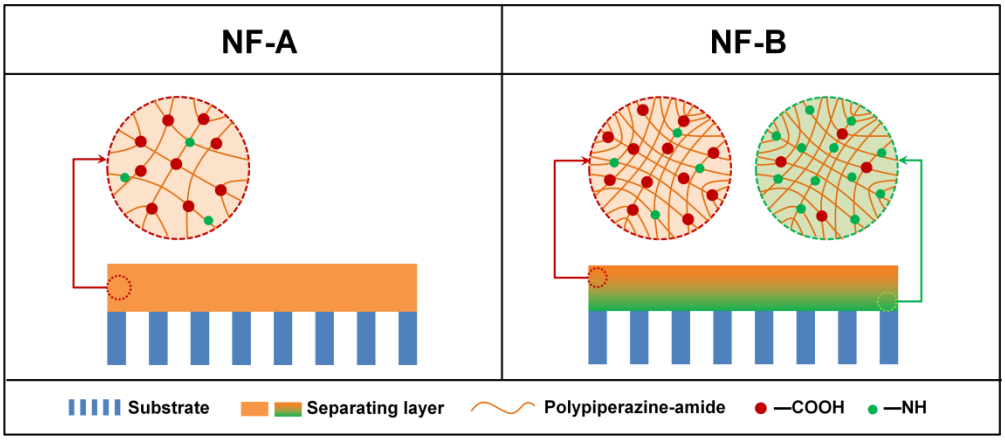

Fig. 2. Configurations of NF-A and NF-B.

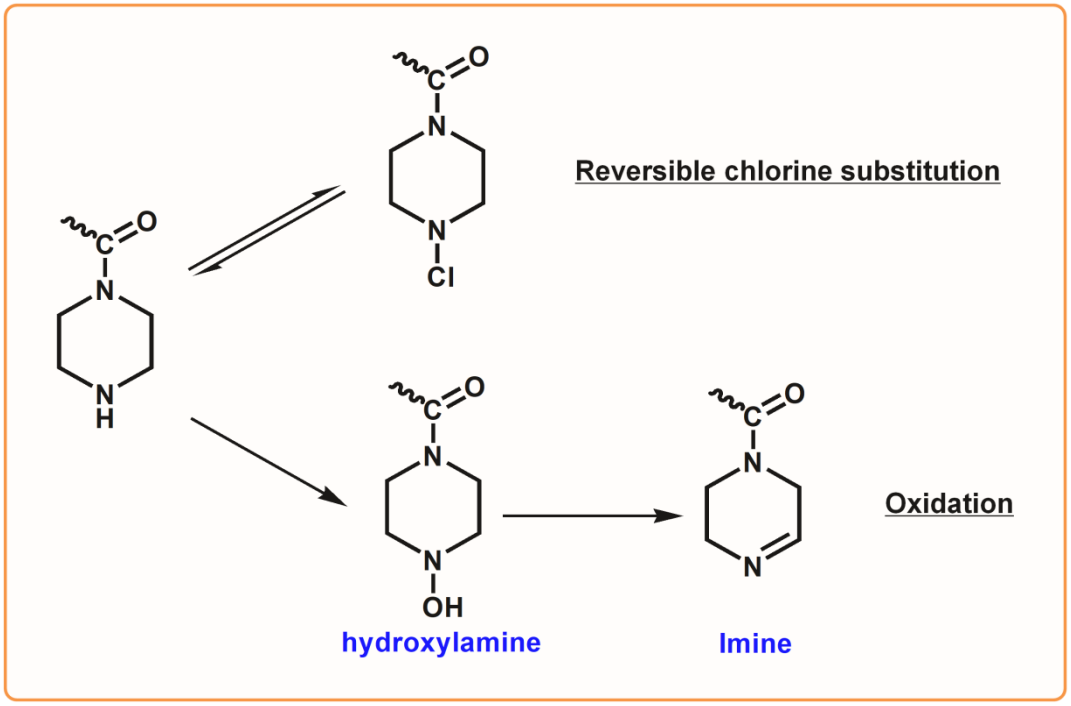

Fig. 3. Possible chlorination mechanism of PPA NFMs.

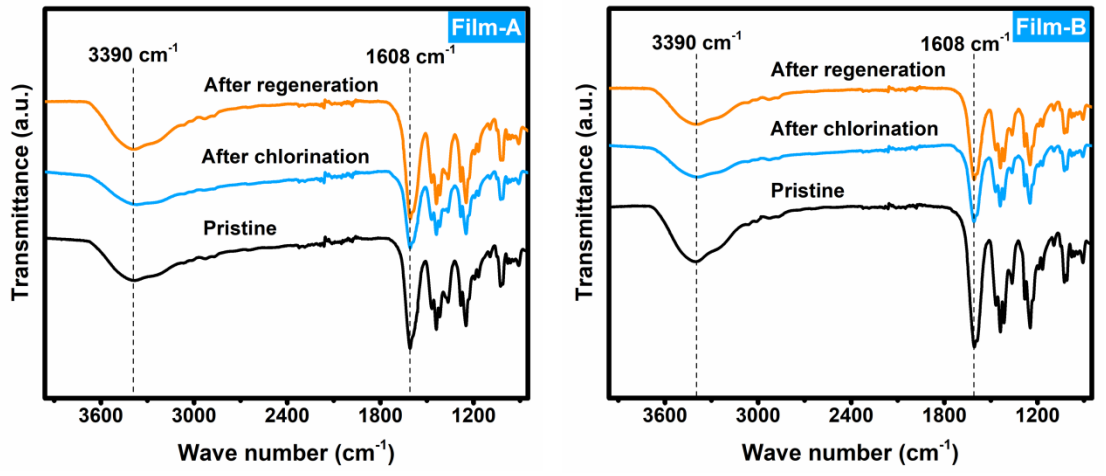

Fig. 4. ATR-FTIR spectra of Film-A and Film-B after chlorination and regeneration. The preparation parameters and treatment processes of Film-A and Film-B (Fig. S2) are similar to that of NF-A and NF-B, respectively. It was believed that the free-standing PPA film had similar physicochemical structure to the PPA separating layer prepared on support membrane.

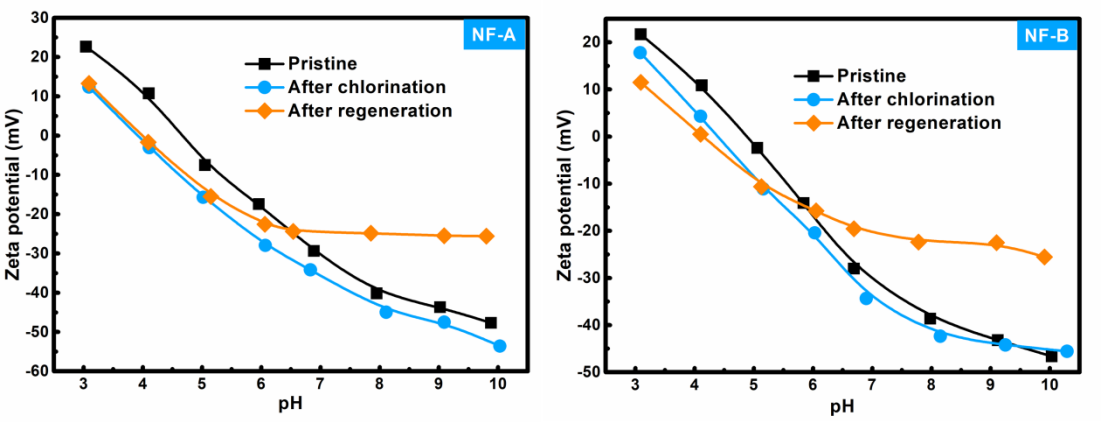

Fig. 5. Zeta potential for pristine, chlorinated and regenerated PPA NFMs as a function of pH.

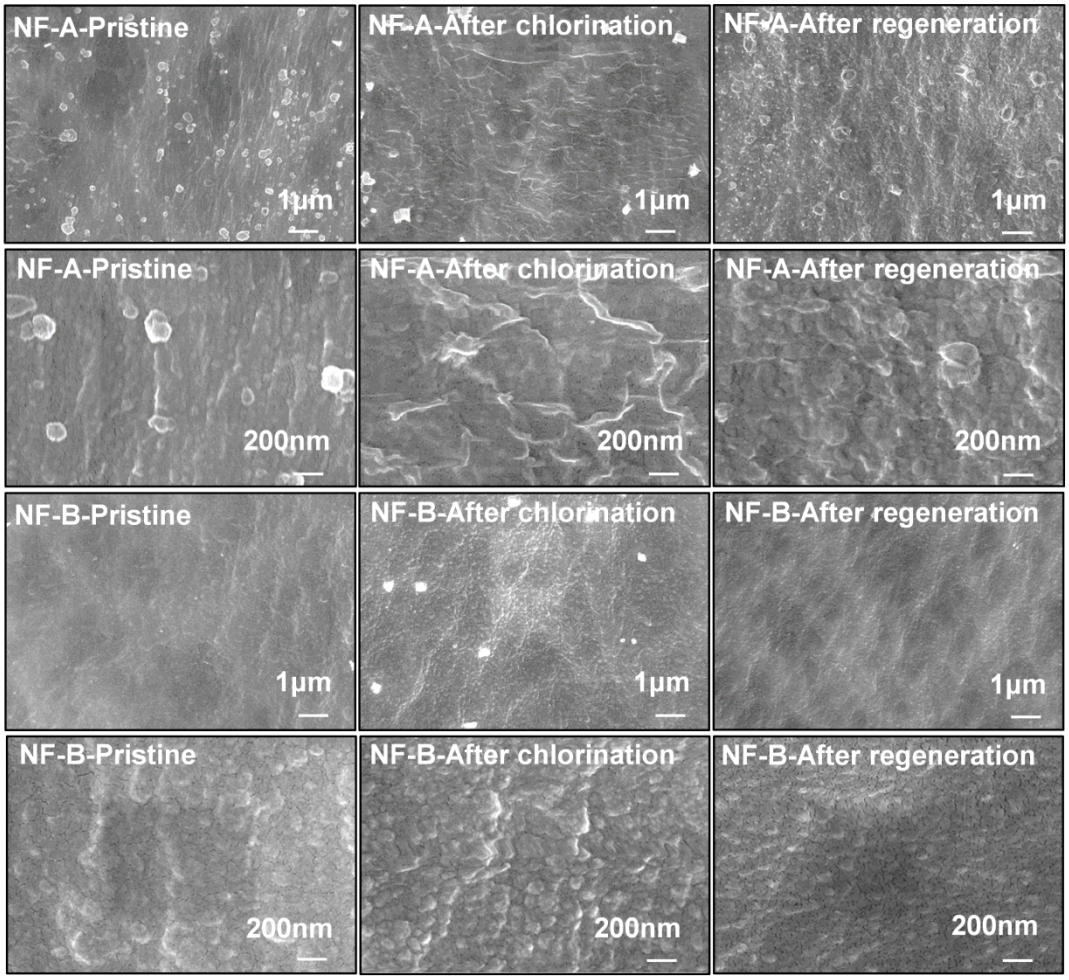

Fig. 6. Top down SEM images of NFMs.

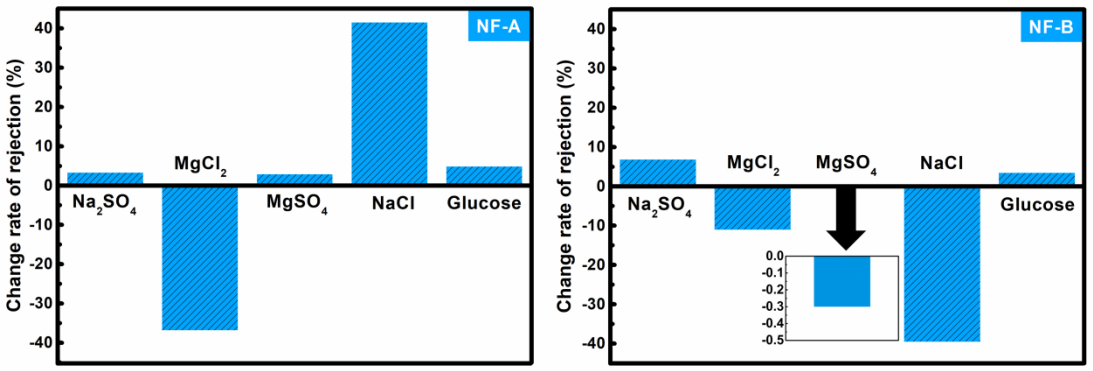

Fig. 7. Change rate of rejections of the selected PPA NFMs after chlorination and regeneration.

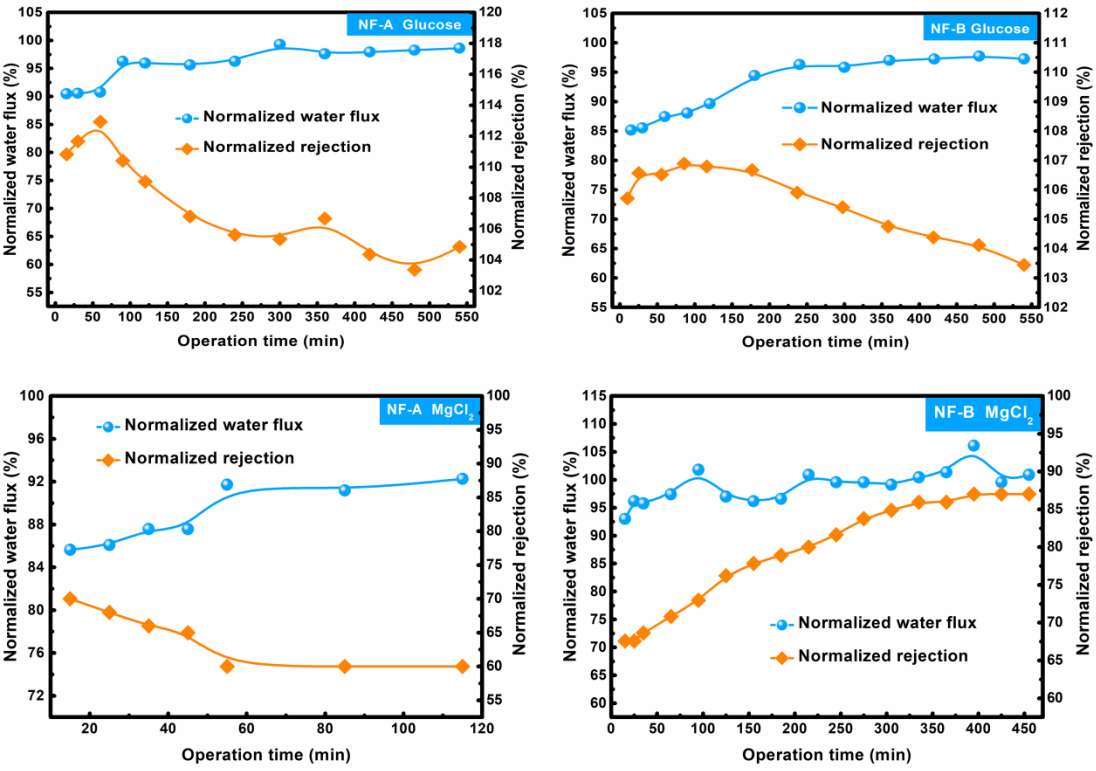

Fig. 8. Water flux and solutes rejection of the two chlorinated PPA NFMs varied with operation time. Test conditions: Glucose concentration = 200 mg·L^{-1}, divalent salts concentration = 1000 mg·L^{-1}, NaCl concentration = 500 mg·L^{-1}, 25 °C, 0.35 MPa.

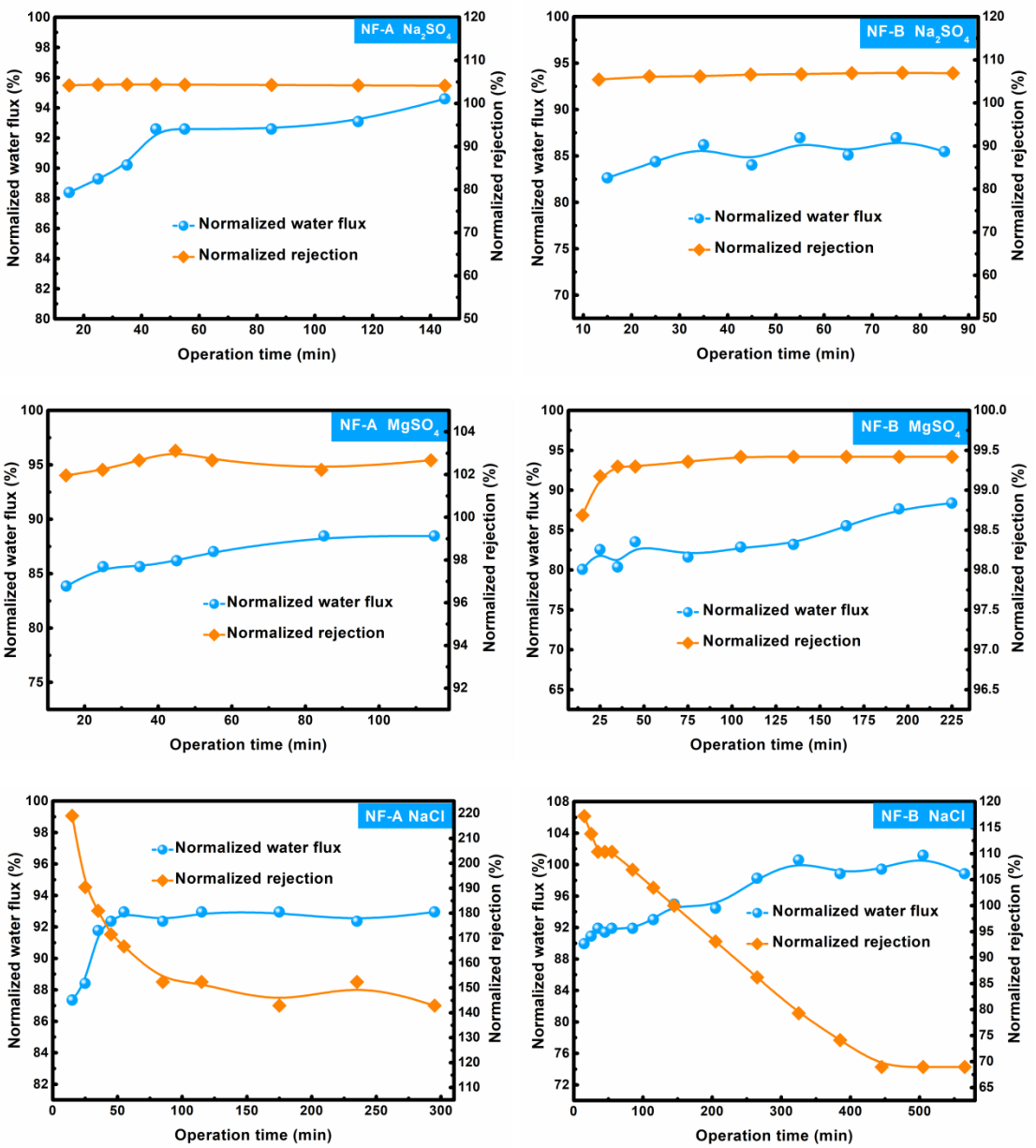

Fig. 8. (*continued*).

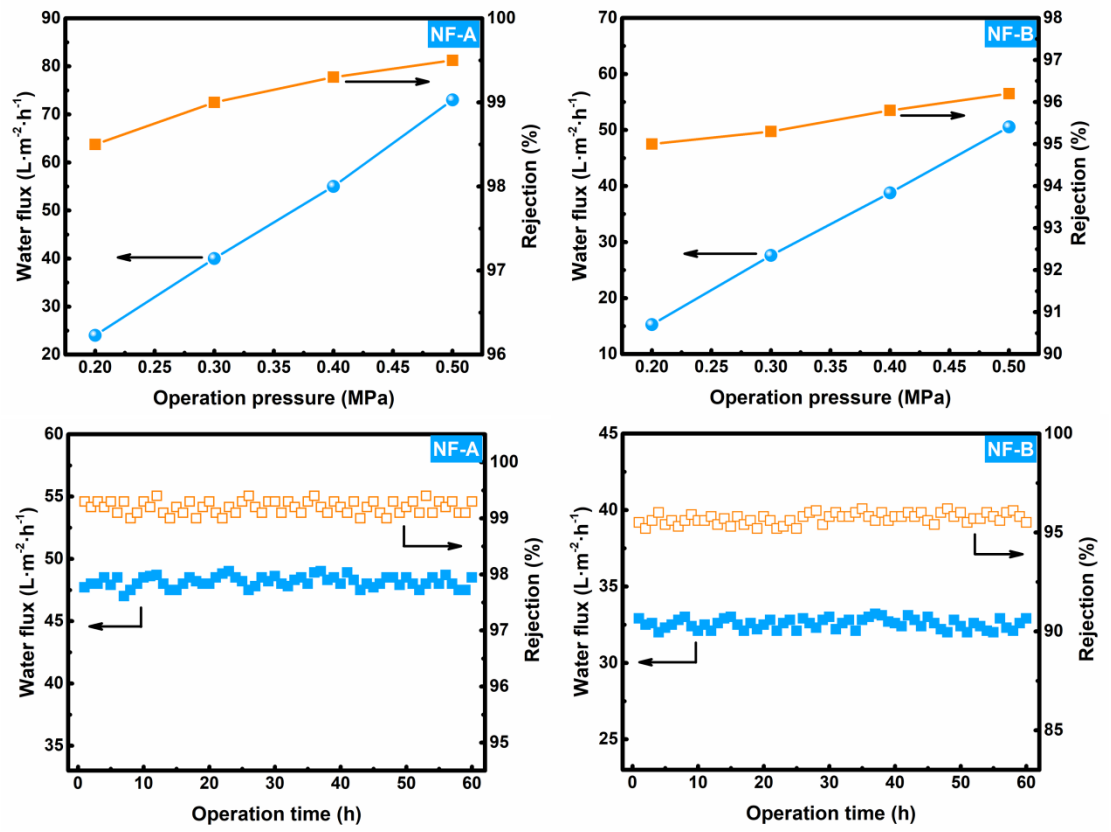

Fig. 9. Structural stability evaluation of the regenerated NF-A and NF-B. Test conditions: Na_2SO_4 concentration = 1000 mg·L^{-1}, 25 °C, 0.35 MPa.

Tables

Table 1 Key preparation parameters of the NFMs used in this work

Membranes	PIP concentration (%)	TMC concentration (%)	Reaction time (s)	Organic phase temperature (°C)
NF-A	0.3	0.3	120	0
NF-B	1.0	0.1	120	0

Table 2 chemical composition changes of the surfaces of the two selected NFMs aroused by chlorination and regeneration

Membranes	Atomic composition (%)				O/N	O/C
	C	N	O	Cl		
NF-A (Pristine)	73.60	9.70	16.70	0.00	1.72	0.23
NF-A (After chlorination)	69.90	10.20	17.70	2.20	1.73	0.25
NF-A (After regeneration)	71.80	10.20	17.30	0.70	1.70	0.24
NF-B (Pristine)	73.60	10.90	15.50	0.00	1.42	0.21
NF-B (After chlorination)	70.40	9.50	18.30	1.80	1.93	0.26
NF-B (After regeneration)	72.00	10.00	17.20	0.80	1.72	0.24

Table 3 Water contact angle for pristine, chlorinated and regenerated PPA NFMs

WCA (°)	Pristine	After chlorination	After regeneration
NF-A	27.6±1.3	22.6±2.4	25.1±1.1
NF-B	48.7±2.8	36.6±3.5	53.0±3.9

Table 4 Original separation performance of the two selected NFMs in this work

Solutes	*R* (%)		*F* ($L \cdot m^{-2} \cdot h^{-1}$)	
	NF-A	NF-B	NF-A	NF-B
Na_2SO_4	95.4±0.9	89.4±1.9	50.4±1.1	38.5±0.3
$MgCl_2$	25.0±1.8	97.8±0.8	56.9±1.2	40.7±3.2
$MgSO_4$	91.4±1.9	99.0±0.5	57.5±0.5	42.1±1.8
NaCl	20.5±0.7	60.7±3.1	61.1±1.0	48.7±2.7
Glucose	67.9±2.0	84.6±2.5	57.5±1.5	45.5±1.2

Test conditions: Glucose concentration = 200 $mg \cdot L^{-1}$, divalent salts concentration = 1000 $mg \cdot L^{-1}$, NaCl concentration = 500 $mg \cdot L^{-1}$, 25 °C, 0.35 MPa.

Supplementary material

Understanding the chlorination mechanism and the chlorine-induced separation performance evolution of polypiperazine-amide nanofiltration membrane

Sihua Liu [a], Chunrui Wu [a,*], Jingguo She [a], Su Liu [b], Xiaotong Hou [a], Xiaolong Lu [a,*], Hongwei Zhang [c], Stephen Gray [d]

[a] *State Key Laboratory of Separation Membranes and Membrane Processes, Institute of Biological and Chemical Engineering, School of Material Science and Engineering, Tianjin Polytechnic University, Tianjin 300387, P. R. China. E-mail: wuchunrui@tjpu.edu.cn (C. Wu), 13920286131@163.com (X. Lu)*

[b] *School of Civil and Environmental Engineering, Georgia Institute of Technology, Atlanta, GA, 30332, United States*

[c] *State Key Laboratory of Separation Membranes and Membrane Processes, School of Environmental and Chemical Engineering, Tianjin Polytechnic University, Tianjin 300387, P. R. China*

[d] *Institute for Sustainability and Innovation, College of Engineering and Science, Victoria University, PO Box 14428, Melbourne, Victoria 8001, Australia*

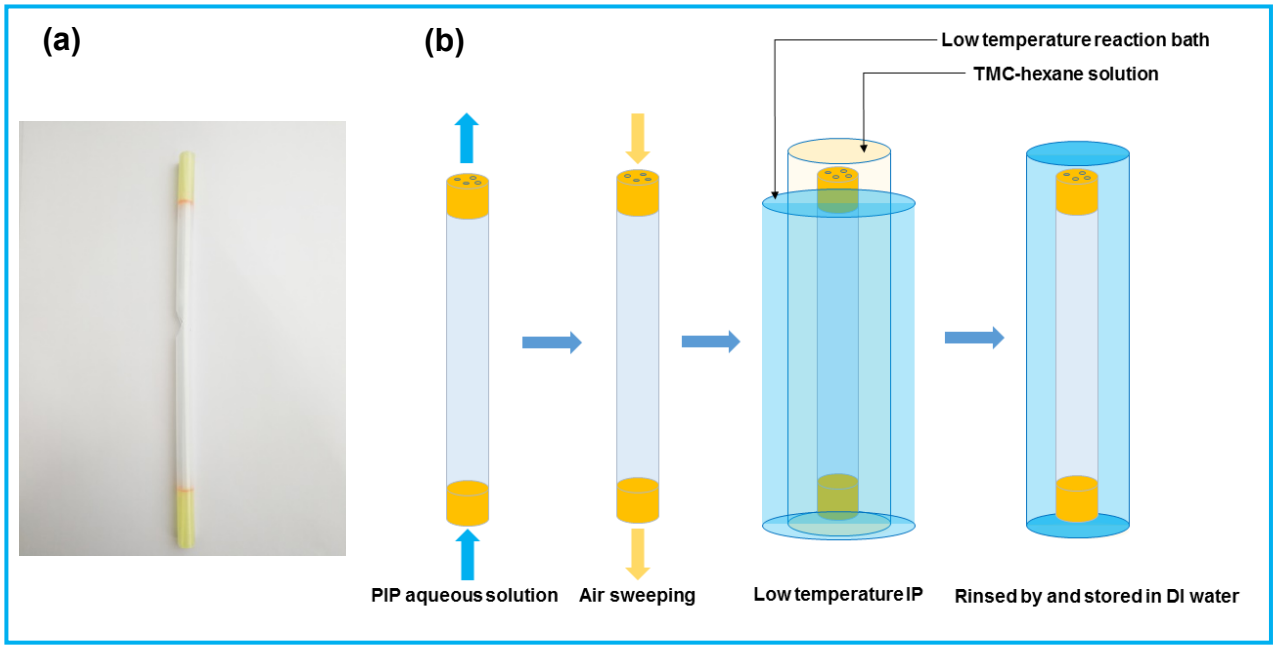

Fig. S1. (a) Digital photograph of hollow fiber membrane module used in this study. (b) Schematic diagram of preparation process of hollow fiber nanofiltration membrane (NFM) via low temperature interfacial polymerization (IP).

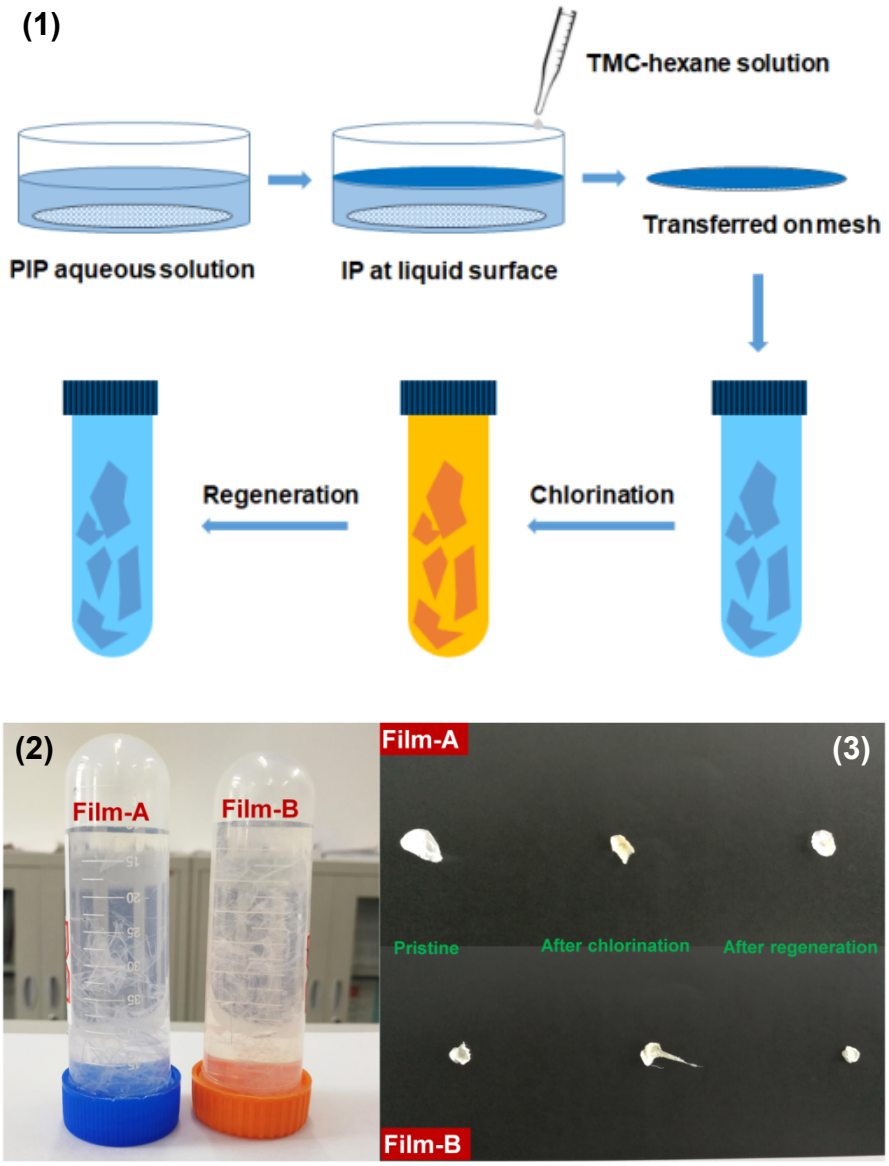

Fig. S2. (1) Schematic diagram of the fabrication and treatment processes of the free-standing polypiperazine-amide (PPA) film. The preparation parameters and treatment processes of Film-A and Film-B are similar to that of NF-A and NF-B, respectively. TMC-hexane solution with a temperature of 0 °C was carefully poured on the surface of PIP aqueous solution (25 °C). After reacting for 120 s, the fabricated free-standing film was collected from the interface by a pre-submerged strainer mesh with a mesh number of 400. The prepared film was dried at 25 °C for 15 min and then transferred into a centrifuge tube containing DI water. The PPA films were conserved in DI water for 3 days and renewed fresh DI water every day. After that, the PPA films were

transferred into a centrifuge tube containing 2000 mg·L^{-1} NaClO solution for 1 hour to conduct the chlorination process. Then, the chlorinated PPA films were rinsed by DI water to remove the absorbed NaClO. To conduct the regeneration process, the chlorinated PPA films were then immersed in DI water for 5 days and renewed fresh DI water every day. Fig S2 (2) Digital photograph of the PPA films in centrifuge tube and the dried samples for ATR-FTIR analysis.

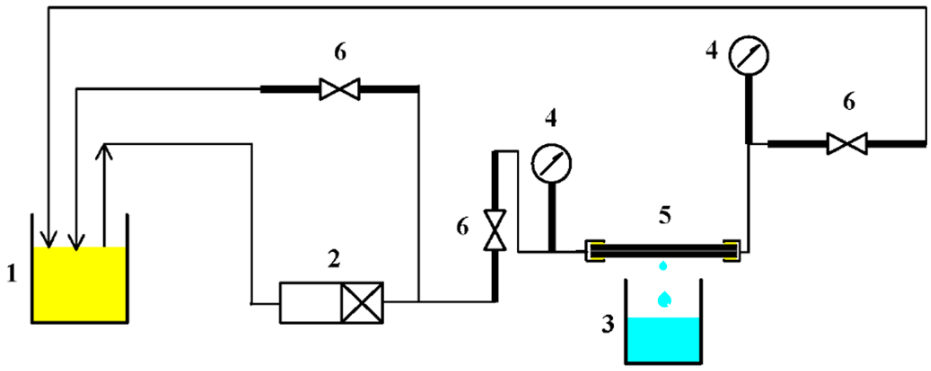

Fig. S3. Schematic diagram of the cross-flow nanofiltration system for hollow fiber modules used in this study.

Table S1. Chemical composition and degree of network cross-linking of NFMs surfaces

Membranes	Atomic composition (%)			O/N	Degree of network cross-linking (%)
	C	N	O		
NF-A	73.60	9.70	16.70	1.72	20.6
NF-B	73.60	10.90	15.50	1.42	47.9

These chemical composition results were acquired from XPS measurements, and the degree of network cross-linking of the NFMs surface were calculated by using the following equation S1 and S2.

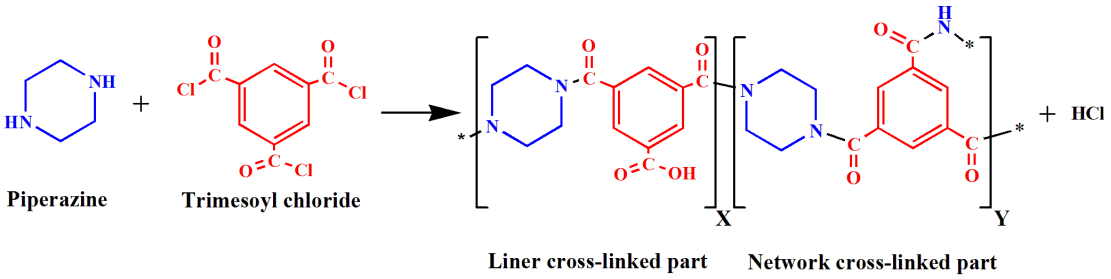

Fig. S4. IP of PIP and TMC and the resultant polymer with liner cross-linked part and network cross-linked part.

$$O/N = \frac{4X + 3Y}{2X + 3Y} \qquad \textbf{Equation S1}$$

$$DNC = \frac{Y}{X + Y} \times 100\,\% \qquad \textbf{Equation S2}$$

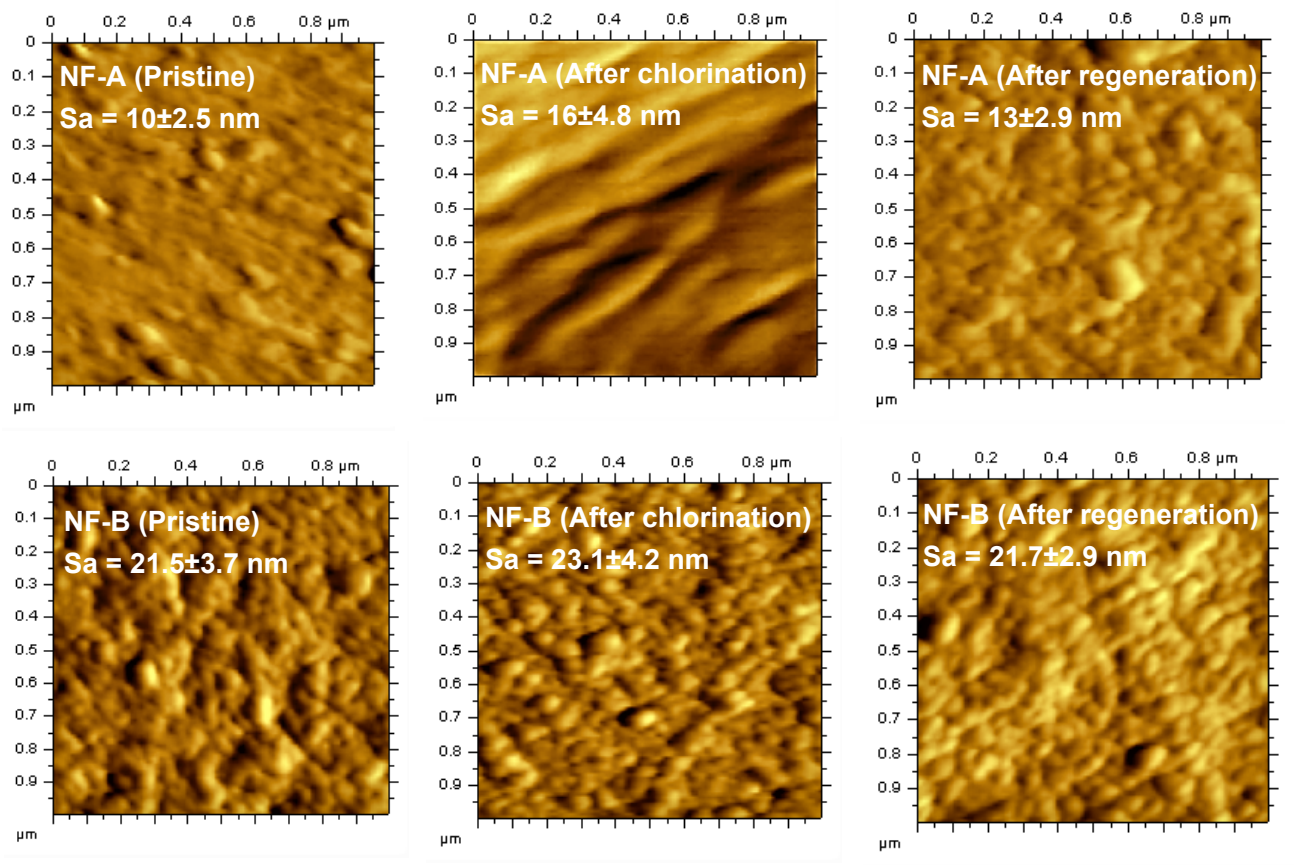

Fig. S5. AFM images of top surface of NFMs. These inserted average roughness data were acquired from AFM measurements over a scanning area of 1 µm by 1 µm. Reported are the averages and standard deviations.